ARTICLE

Effects of Oxide Platforms on the Dynamics and Reduction Characteristics of Hydrogen Spillover

Received 00th January 20xx,
Accepted 00th January 20xx

DOI: 10.1039/x0xx00000x

Kazuki Shun,[a] Akihito Fujimoto,[a] Kohsuke Mori, *[ab] and Hiromi Yamashita [ab]

The characteristics of hydrogen spillover on various metal oxides, involving the concurrent diffusion of protons (H^+) and electrons (e^-), were systematically studied by combining *in situ* analytical techniques with kinetic analyses. H_2-temperature programmed reduction and *in situ* X-ray absorption fine structure data showed that hydrogen spillover from Pt onto TiO_2 and WO_3 greatly decreased the temperatures at which Zn^{2+} ions deposited on these remote metal oxides were reduced. In contrast, hydrogen spillover on MgO and CeO_2 did not significantly affect the reduction of remote Zn^{2+}. Mechanisms explaining the effects of spilled hydrogen on reduction for each oxide substrate were proposed based on the dynamic behaviors of H^+ and e^- as ascertained by means of *in situ* spectroscopic characterizations and kinetic analyses. The results of this work indicate that e^- diffusion rather than H^+ diffusion promotes the reduction of deposited metal ions and that interparticle hydrogen spillover can be facilitated over TiO_2 and WO_3 as a consequence of the interfacial diffusion of H^+ and e^- pairs. These findings provide an improved understanding of the hydrogen spillover phenomenon.

Introduction

Hydrogen spillover is a dynamic phenomenon involving the diffusion of coupled protons (H^+) and electrons (e^-).[1-3] This phenomenon is initiated by the production of atomic hydrogen from gaseous H_2 on noble metal nanoparticles such as Pt, Pd, and Ru followed by their migration onto the support materials[4]. Subsequently, the atomic hydrogen forms the H^+ and e^- pairs and diffuses on the supports driven by increasing configurational surface entropy.[5] The occurrence of hydrogen spillover has the potential to enhance the performance of materials employed in catalysis,[6-8] hydrogen storage[9-11] and fuel cells.[12-14] One notable feature responsible for these promotional effects is the exceptional reducing power of so-called spilled hydrogen, which enables the simultaneous and uniform reduction of multiple metal ions having distinct reduction potentials.[15, 16] By taking advantage of this characteristic, advanced multicomponent nanoparticles, such as high-entropy alloys and binary alloys with positive mixing enthalpies, can be synthesized at mild heating rates and at relatively low temperatures.[17-19]

There have recently been many studies of hydrogen spillover dynamics with the aim of establishing a theoretical basis for this phenomenon.[20-22] Karim and colleagues reported that spilled atomic hydrogen generated on Pt particles on Al_2O_3 can spill only within a 15 nm radius, whereas migration as far as 1 µm is possible on TiO_2.[23] Our own group has demonstrated that spilled atomic hydrogen migrates more readily on TiO_2 and CeO_2 surfaces but moves into the bulk region of WO_3.[24] These different behaviors are attributed to variations in the reducibility of the platform materials.[25] On this basis, readily reducible metal oxides such as TiO_2, CeO_2 and WO_3 are recognized as promising platforms for hydrogen spillover while non-reducible metal oxides, including MgO, Al_2O_3 and SiO_2, tend to restrict the dynamics of spilled atomic hydrogen.[26-28] Intriguingly, its effect have been reported to extend outside the oxide particles where noble metal deposited.[29, 30]

Although various insights into spilled atomic hydrogen dynamics have been accumulated, the reduction characteristics associated with spillover remain poorly understood. However, it has been reported that the reduction of deposited metal ions is significantly promoted on reducible metal oxides,[23, 27] suggesting that the reduction behavior of spilled atomic hydrogen is also governed by the reducibility of the platform. In fact, the electronic state of spilled atomic hydrogen is determined by the ability of the metal oxide to allow the redox reaction of cations. During spillover, H^+-e^- pairs are generated on reducible metal oxides according to the reaction $M^{n+} + O^{2-} + H \rightarrow M^{(n-1)+} + OH^-$, whereas only H^+ diffuses on non-reducible metal oxides because these compounds inhibit the diffusion of e^-.[3, 31] Accordingly, the hydrogen spillover on reducible metal oxides and the H^+ diffusion on non-reducible metal oxide are different in the terms of the electronic state of spilled atomic hydrogen. For these reasons, the reduction behavior associated with spilled hydrogen on a given metal oxide can be investigated by assessing the dynamic behaviors of H^+ and e^- on that compound.

The present work studied the reduction characteristic of spilled hydrogen on various oxides by examining the dynamics of H^+ and e^-, employing physical mixtures of Pt and Zn^{2+} supported on various materials as specimens. The results provide two general insights concerning hydrogen spillover. Firstly, the reduction characteristics

[a] *Division of Materials and Manufacturing Science, Graduate School of Engineering, Osaka University, 2-1 Yamadaoka, Suita, Osaka 565-0871, Japan. E-mail: K. M. mori@mat mat.eng.osaka-u.ac.jp*
[b] *Innovative Catalysis Science Division, Institute for Open and Transdisciplinary Research Initiatives (ICS-OTRI), Osaka University, Suita, Osaka 565-0871, Japan.*

Supplementary Information available: [details of any supplementary information available should be included here]. See DOI: 10.1039/x0xx00000x

of spilled atomic hydrogen are evidently affected by e^- diffusion rather than H^+ diffusion. Secondly, the reduction of metal ions can be facilitated by interparticle hydrogen spillover over TiO_2 and WO_3 owing to the readily interfacial diffusion of H^+ and e^- pairs on these oxides. This study provides practical insights and new guidelines for the design of technologies based on hydrogen spillover.

Results & Discussion

Zn^{2+} reduction characteristics on each metal oxide

In order to investigate the effect of hydrogen spillover on the Zn^{2+} reduction characteristics, we contacted Pt^{4+} and Zn^{2+} ions by the physically mixing of Pt/MO_x and Zn/MO_x based on the physical mixture strategy employed in previous work.[32, 33] TEM results of synthesized (Pt + Zn)/MO_x specimens showed the agglomerated large secondary particles composed of small primary particles, which demonstrates that physically mixed Pt/MO_x and Zn/MO_x are in good contacted with each other, allowing hydrogen spillover from Pt to Zn through their supports (Figure S1). It has previously reported that the occurrence of hydrogen spillover significantly lowers the reduction temperature of deposited metal ions compared with the reduction by the H_2 molecules.[16, 17, 23] Stated differently, the effects of platform oxides on the reduction characteristic of spilled hydrogen can be evaluated by comparing the reduction temperatures of deposited metal ions in the absence and presence of noble metal nanoparticles initiating hydrogen spillover. Herein, H_2-TPR data were collected to examine the reduction behavior of Zn^{2+} ions ($E_0(Zn^{2+}/Zn)$ = -0.763 V vs. NHE) contained in Zn/MO_x and in physically mixed (Pt + Zn)/MO_x specimens (Figure 1). In the resulting plots, H_2 consumption events contain the reduction of the specimen (i.e. the reduction of deposited ions and the support material) appear as peaks. Each specimen was exposed to the H_2 contained atmosphere prior to H_2-TPR trials which stabilizes TCD signal. It has been reported that Pt ions reduced below 30 °C,[34] and therefore each H_2 consumption in H_2-TPR profiles exhibits the reduction of either Zn ions or MO_x. The Zn/MgO generated single peaks associated with reduction at 359 and 340 °C in the absence or presence of Pt, respectively. This result suggests that the reduction behavior of Zn^{2+} did not change even though the Pt was able to promote the dissociation of H_2 molecules. In prior studies, spilled atomic hydrogen diffusing over non-reducible metal oxides such as MgO and Al_2O_3 were found not to significantly affect the reduction of metal cations, consistent with the present work.[17, 27] In contrast, the reduction temperature shown by the Zn/TiO_2 was decreased by 159 °C in the presence of Pt, demonstrating the ability of H^+-e^- pairs on a reducible metal oxide to promote the reduction of metal cations, as has been previously reported.[17, 27] Surprisingly, the reduction temperature for the Zn/CeO_2 was decreased by only 17 °C following the incorporation of Pt, and so was similar to the value for the non-reducible oxide MgO even though CeO_2 is typically considered a reducible metal oxide. Moreover, the reduction of Zn^{2+} ions and CeO_2 in (Pt + Zn)/CeO_2 almost coincided which suggests that the reduction characteristic of hydrogen spillover on CeO_2 is associated with the reduction of CeO_2. In the case of the Zn/WO_3, the reduction temperature was decreased by 92 °C in the presence of Pt, again demonstrating a promotional effect. It should be noted that the reduction temperature of Zn^{2+} on (Pt + Zn)/MgO did not significantly decrease even though the specific surface area of MgO is much smaller than that of TiO_2 where Zn^{2+} ion was promotionally reduced under co-existence of Pt. These results indicate that the reduction characteristic of hydrogen spillover is not affected by the distance between Pt and Zn ions. It is evident from these results that the reduction behaviors of spilled atomic hydrogen species differed between those samples made using non-reducible and reducible metal oxides but also even between the different reducible metal oxides. Because hydrogen spillover involves the concurrent diffusion of H^+ and e^-, the dynamic behaviors of both charged particles on each metal oxide were assessed based on a combination of *in situ* techniques, so as to examine the driving forces for these processes.

Dynamic behavior of spilled atomic hydrogen on MgO

The characteristics of spilled hydrogen on non-reducible metal oxides such as Al_2O_3 and MgO have been widely studied[26, 35] and some such studies have reported inferior reduction properties compared with reducible metal oxides. [23, 28] Hence, the research reported herein observed the behavior of spilled hydrogen species on MgO to elucidate the origin of the reduction properties of this material. *In situ* Zn K edge XAFS data were acquired under a D_2 atmosphere at elevated temperatures in trials with both the Zn/MgO and (Pt + Zn)/MgO (Figure 2a). In contrast to the H_2-TPR analyses, which provided information concerning the reduction behaviors of both the Zn^{2+} ions and platform oxide, the XAFS assessments only monitored the oxidation state of the Zn^{2+} ions. The results indicate that the attenuation of the white line generated by the (Pt + Zn)/MgO was similar to that for the Zn/MgO, suggesting that the presence of Pt did not significantly affect the reduction behavior of the Zn^{2+}, in agreement with the H_2-TPR findings (Figure 1). The intensity of white line attenuated in accordance with the transition of E_0 position during the reduction treatment (Figure S2). The behavior of spilled

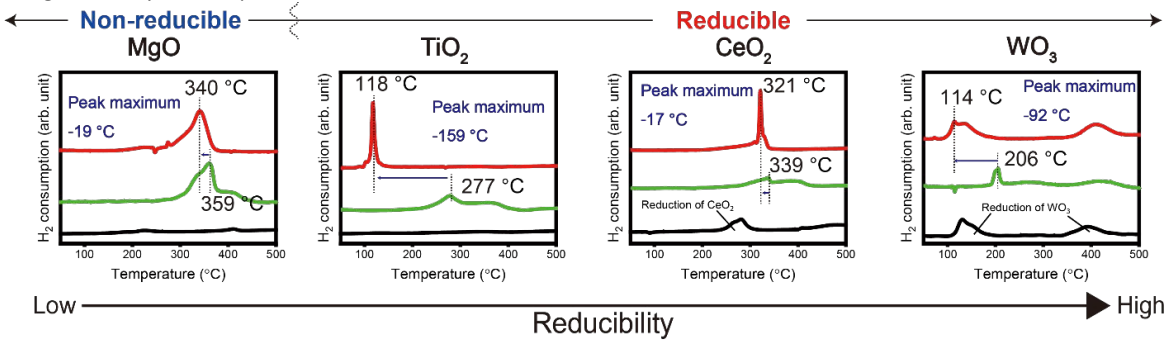

Figure 1. H_2-TPR profiles for Pt/MO_x (black), Zn/MO_x (green), and (Pt + Zn)/MO_x (red) specimens at a heating rate of 5 °C/min.

atomic hydrogen on the MgO substrate was also examined by acquiring *in situ* DRIFT spectra under D_2 in conjunction with the XAFS experiments (Figure 2b). In the resulting spectra, the diffusion of D^+ ions can be monitored by observing the peaks related to O^{2-}–D^+ stretching vibrations (δ_{O-D}) in the range of 2800-2600 cm^{-1}.[36, 37] It should be noted that this peak evolved during D_2 dosage and attenuated during H_2 dosage which demonstrates that the δ_{O-D} was evolved by the proton diffusion phenomenon (Figure S3). The dominant δ_{O-D} peak was observed at 150 °C, confirming that proton diffusion readily took place over the MgO at temperatures above 150 °C. This temperature range is lower by 80 °C compared with that for the onset of the reduction of the deposited Zn^{2+}, as demonstrated by the E_0 transition in the Zn K edge XANES spectra shown in Figure 2c. It should be noted that the electronic state of reduced Zn is not related to the effect of hydrogen spillover, but is affected by the acid-base property of the support materials,[38] therefore we herein assessed at what temperature the E_0 of XANES start to shift. In this way, the E_0 transitions for the Zn/MgO and (Pt + Zn)/MgO were observed within almost the same temperature ranges (Figure S4). That is, spilled atomic hydrogen on MgO did not significantly promote the reduction of deposited Zn^{2+} ions. It has previously been reported that dissociated atomic hydrogen diffuses as H^+ over non-reducible metal oxides because the cations of these oxides are too irreducible to accept e^-, meaning that e^- diffusion is inhibited.[26] Thus, the inhibited reduction of deposited Zn^{2+} on MgO as observed in this work is attributed to the fact that H^+ ions were not accompanied by e^- due to the low reducibility of cations in the MgO. The dynamic behaviors of H^+ and e^- on reducible metal oxides whose cations are relatively easy to reduce were subsequently investigated to obtain additional insights.

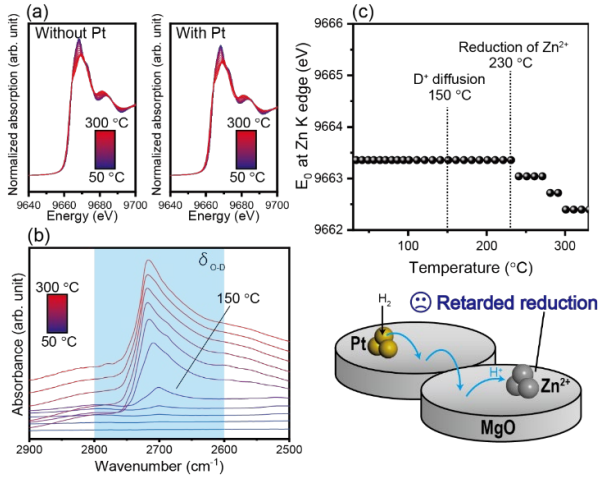

Figure 2. (a) Zn K edge *in situ* XANES spectra of Zn/MgO (left) and (Pt + Zn)/MgO (right) obtained under D_2 at various temperatures. (b) *In situ* DRIFT spectra of (Pt + Zn)/MgO acquired under D_2 at various temperatures. (c) The E_0 transition in the XANES data within the Zn K edge region for (Pt + Zn)/MgO during D_2 reduction (top) and the proposed dynamic behavior of atomic hydrogen species spilled on MgO (bottom).

Dynamic behavior of hydrogen spillover on TiO_2

Hydrogen spillover on TiO_2 is known to have a strong reducing effect and so this effect is widely utilized in a variety of functional catalysts.[32, 39, 40] Even so, there are insufficient experimental data concerning the origin of this reduction behavior. The present work therefore examined the manner in which hydrogen spillover on TiO_2 affected the reduction of Zn^{2+} ions. In the case of the *in situ* Zn K edge XANES spectra acquired under D_2 at elevated temperatures, the white line intensity generated by the (Pt + Zn)/TiO_2 was rapidly attenuated at approximately 50 °C whereas the intensity for the pure Zn/TiO_2 gradually decreased as the temperature was increased (Figure 3a). Additionally, the E_0 transitions for the (Pt + Zn)/TiO_2 were observed at lower temperature range than Zn/TiO_2 (Figure S5). These results demonstrated that hydrogen spillover on the TiO_2 contributed to the reduction of the Zn^{2+} ions, which was consistent with the H_2-TPR data (Figure 1a). The dynamic behaviors of D^+ and e^- were investigated by obtaining *in situ* DRIFT spectra under D_2 (Figure 3b). Above 80 °C, a δ_{O-D} peak associated with D^+ diffusion was observed in the (Pt + Zn)/TiO_2 spectra. It can be assumed that the broadening of the δ_{O-D} peak represents the inhomogeneity of the O^{2-}–D^+ dipole state derived from oxygens in various coordination states. On the other hand, an intense peak appeared at 1300 cm^{-1} in the spectra acquired at temperatures as low as 30 °C. It was previously reported that an e^- generated by hydrogen spillover was transferred to the midgap states (MGSs) below conduction band (CB) of TiO_2 and excited from MGSs to CB by an irradiation of infrared light.[41, 42] We have previously observed a broad IR absorption band in a range of 2000–1000 cm^{-1} for Pt/TiO_2 under H_2 reduction condition, corresponding to e^- diffusion via MGS driven by hydrogen spillover.[43] Considering the decrease in absorbance in the range of 1600-1400 cm^{-1}, which was attributed to the desorption of H_2O and HOD at elevated temperatures,[36] the peak observed in the present work can be assigned to the trapping of e^- in MGSs located below the TiO_2 conduction band. Presumably, e^- were able to diffuse over the TiO_2 at temperatures as low as 30 °C even though the δ_{O-D} peak was only observed above 80 °C, suggesting that e^- diffusion was preceded by H^+ diffusion. Moreover, as shown in Figure 3c, the E_0 transition in the Zn K edge XANES spectra resulted not from H^+ diffusion but rather from e^- diffusion. Consequently, it is likely that the diffusion of e^- (rather than that of H^+) over the TiO_2 enhanced the reduction of Zn^{2+}, which also explains the retarded reduction of Zn^{2+} on MgO. Based on the results for MgO and TiO_2, it can be estimated that the dynamic behavior of e^- has a greater effect on the reduction behavior of spilled atomic hydrogen than that of H^+.

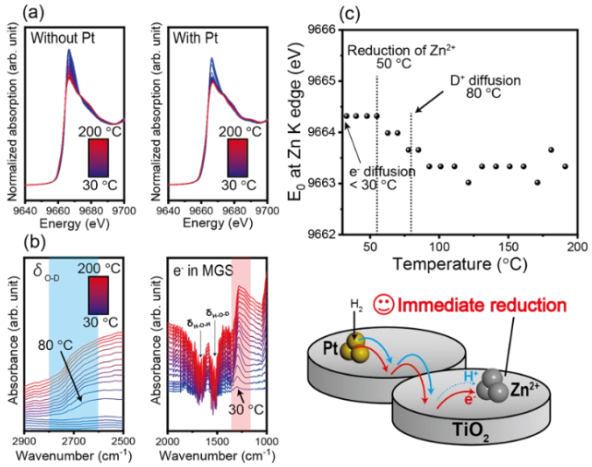

Figure 3. (a) Zn K edge *in situ* XANES spectra obtained from Zn/TiO_2 (left) and (Pt + Zn)/TiO_2 (right) under D_2 at various temperatures. (b) *In situ* DRIFT

spectra obtained from (Pt + Zn)/TiO_2 under D_2 at various temperatures, showing the regions associated with O-D bonding (left) and e^- in MGSs (right). (c) The E_0 transition of the XANES data within the Zn K edge region for (Pt + Zn)/TiO_2 under D_2 (top) and the proposed dynamic behavior of atomic hydrogen species spilled on TiO_2 (bottom).

Dynamic behavior of hydrogen spillover on CeO_2

CeO_2 is a promising platform material for catalysts due to the exceptional redox properties and shape-controllable nature of this material.[44] The hydrogen spillover characteristics of this oxide have also been examined in recent years because this phenomenon can greatly improve the performance of various catalysts.[45, 46] The present work assessed the reduction performance of CeO_2 in terms of the dynamics of H^+ and e^- diffusion and the associated effects on the reduction of deposited ions. *In situ* DRIFT data were obtained to monitor the dynamics of H^+ and e^- on (Pt + Zn)/CeO_2 (Figure 4a). The appearance of a δ_{O-D} peak attributable to D^+ diffusion on the CeO_2 substrate was observed above 150 °C, as has been previously reported.[24] Notably, this peak sharpened above 300 °C, indicating an increase in the intensity of O^{2-}–D^+ stretching vibrations and the homogenization of the O^{2-}-D^+ dipole states owing to the surface relaxation of CeO_2 surface.[45] A peak related to the evolution of Ce^{3+} was also observed around 2100 cm^{-1} at temperatures above 250 °C.[47, 48] The formation of Ce^{3+} is associated with a continuous e^- donation from hydrogen to Ce^{4+}. These results demonstrate that hydrogen spillover involving the concomitant diffusion of H^+ and e^- pairs took place on (Pt + Zn)/CeO_2 at about 250 °C, even though Zn^{2+} ions on (Pt + Zn)/CeO_2 did not undergo reduction below 300 °C (Figure 1). To obtain information concerning the thermodynamics of hydrogen spillover on CeO_2, the activation energies for the reduction of Zn^{2+} (E_a) on the (Pt + Zn)/MO_x specimens (MO_x = TiO_2, CeO_2 or WO_3) were evaluated using the Kissinger equation based on H_2-TPR data generated at various heating rates (Figure 4b and Figures S6 and S7).[49] Interestingly, the E_a for CeO_2 was calculated to be 96.5 kJ/mol and so was more than 70 kJ/mol greater than the values for TiO_2 and WO_3. It can be assumed that the rate-determining step for the reduction of Zn^{2+} by hydrogen spillover from Pt deposited on the remote platform was specific for CeO_2. Another possibility is that spilled H^+-e^- pairs on the CeO_2 were less reductive than those on other reducible metal oxides. To clarify this, additional H_2-TPR data were acquired for a specimen in which Pt^{4+} and Zn^{2+} were both loaded on CeO_2 (Figure S8). Interestingly, a peak attributable to the reduction of Zn^{2+} appeared between 150 and 250 °C even though Zn^{2+} deposited on (Pt + Zn)/CeO_2 was only reduced above 300 °C. This result demonstrates that intraparticle hydrogen spillover took place on the CeO_2 above 150 °C and that the spilled H^+-e^- pairs on this substrate were able to reduce Zn^{2+} at a lower temperature compared with the temperature required for reduction by gaseous H_2. It is therefore evident that intraparticle hydrogen spillover on the CeO_2 was the rate-determining step for the reduction of Zn^{2+} deposited on this material. This explains the sharp δ_{O-D} peak in Figure 4a, which resulted from interparticle hydrogen spillover from Pt/CeO_2 to Zn/CeO_2. This spillover increased the total number of O^{2-}–D^+ bonds on the (Pt + Zn)/CeO_2. Lee and coworkers previously demonstrated that the formation of Ce^{3+} in response to H_2 exposure was facilitated in a mixture of CeO_2 loaded with Pt and pure CeO_2 following reduction under H_2 at 400 °C. This effect occurred because boundaries formed between CeO_2 particles provided pathways for interparticle hydrogen spillover due to sintering in the initial reducing H_2 atmosphere.[45] This insight also suggests that interparticle hydrogen spillover, the driving force for the reduction of Zn^{2+} ions remote from Pt on the substrate, will only occur at high temperature on pristine CeO_2 because of a lack of such boundaries at low temperatures. The reduction characteristics and dynamics of spilled hydrogen on CeO_2 are depicted diagramatically in Figure 4c. Intraparticle hydrogen spillover involving the diffusion of H^+ and e^- was observed on CeO_2 loaded with Pt above 250 °C. However, the reduction of Zn^{2+} deposited on remote CeO_2 was negligible up to 250 °C where intraparticle hydrogen spillover occurred because interparticle hydrogen spillover was prohibited. At approximately 300 °C, boundaries evolved between CeO_2 particles that provided hydrogen spillover pathways from Pt to Zn^{2+} due to the sintering of the oxide.

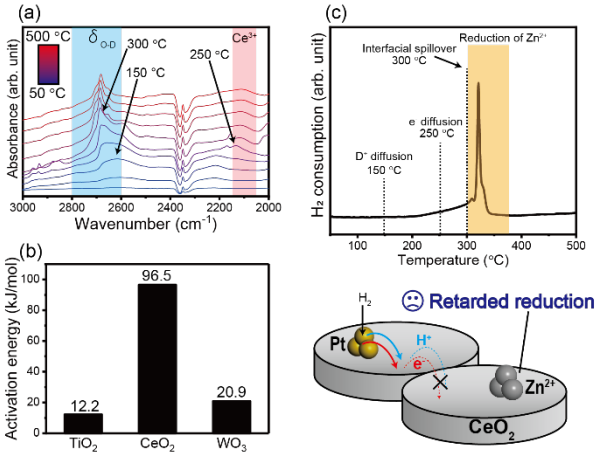

Figure 4. (a) *In situ* DRIFT spectra acquired from (Pt + Zn)/CeO_2 under D_2 at various temperatures showing the O-D (blue) and Ce^{3+} (right) regions. (b) Activation energies for the reduction of Zn^{2+} in each (Pt + Zn)/MO_x specimen as calculated based on Kissinger plots. (c) The H_2-TPR profile obtained for (Pt + Zn)/CeO_2 labeled to indicate hydrogen spillover and the reduction of Zn^{2+} (top) and the proposed dynamic behavior of atomic hydrogen species spilled on CeO_2 (bottom).

Dynamic behavior of hydrogen spillover on WO_3

Hydrogen spillover on WO_3 has been known for over 50 years and has been employed to produce photo- and electrocatalysts.[1, 50, 51] This phenomenon can facilitate the reduction of deposited metal ions[24] although the origin of the driving force for this process remains unclear. Herein, the reduction behavior of hydrogen spillover is disentangled from the dynamics of H^+ and e^- diffusion. *In situ* XAFS measurements for Zn/WO_3 and (Pt + Zn)/WO_3 demonstrated the promoted reduction of Zn^{2+} under the co-existence of Pt (Figure S9), which is consistent to the tendency of H_2-TPR. Therefore, the hydrogen spillover, the simultaneous diffusion of H^+ and e^-, on WO_3 can behave as a strong reduction agent. The H^+ diffusion characteristics on WO_3 were investigated by monitoring the evolution of the δ_{O-D} peak in *in situ* DRIFT spectra acquired under D_2 (Figure 5a). An intense δ_{O-D} peak appeared at 100 °C that was related to H^+ diffusion on the surface of the WO_3. We previously reported

that H^+ preferentially diffuses into the bulk region rather than the surface in the case of WO_3.[24] Therefore, H^+ ions likely diffused into the WO_3 below 100 °C. Note that the decay of this δ_{O-D} peak may have been due to the formation of D_2O as a consequence of the condensation of O−D groups on the surface.[52] The extent of e^- diffusion over the (Pt + Zn)/WO_3 surface was also studied by acquiring *in situ* UV-visible spectra under H_2, as shown in Figure 5b. The WO_3 was found to change color from yellow to bronze upon accepting e^- based on mixing of the W^{6+} and W^{5+} valence transfer bands. Thus, the visible light absorption of this specimen could be utilized to study hydrogen spillover, meaning coupled H^+ and e^- diffusion.[53, 54] The WO_3 exhibited visible light absorption based on the formation of W^{5+} above 50 °C, providing evidence for e^- diffusion. Considering that H^+ diffusion occurred below 100 °C, hydrogen spillover involving simultaneous H^+ and e^- diffusion appears to have taken place on this oxide beginning at approximately 50 °C. The absorption of visible light was found to decrease beginning at 75 °C with no increases from 100 to 175 °C, confirming the competitive supply and consumption of e^- on the WO_3. The temperature region where visible light absorption by WO_3 did not increase in the *in situ* UV-vis spectra corresponds to that where the reduction peak was observed in the H_2-TPR data (Figure 5c). From these results, it can be assumed that the diffusion of H^+-e^- pairs over the WO_3 was responsible for the reduction of Zn^{2+}. Hydrogen spillover on WO_3 was evidently slower than that on TiO_2 because there was no increase in the visible light absorbance of WO_3 during the reduction of Zn^{2+}, presumably because the greater reducibility of W^{6+} resulted in the capture of e^-.

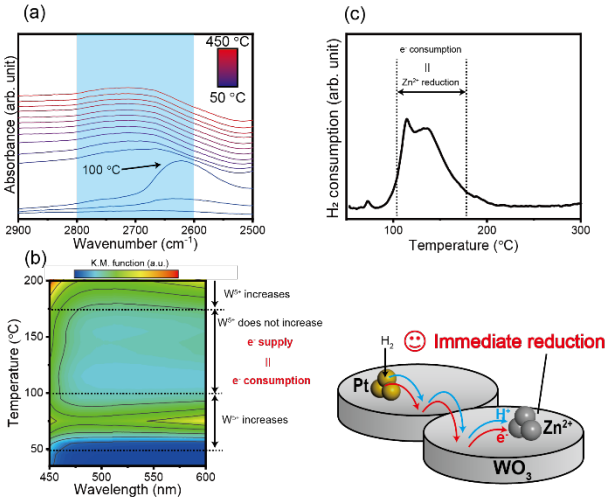

Figure 5. (a) *In situ* DRIFT spectra acquired from (Pt + Zn)/WO_3 under D_2 at various temperatures in the O-D region. (b) Visible light absorption data showing the presence of W^{5+} within a Pt/WO_3 specimen as obtained by an *in situ* UV-visible method during reduction under H_2. (c) The H_2-TPR profile obtained for (Pt + Zn)/WO_3 labeled to indicate hydrogen spillover and the reduction of Zn^{2+} (top) and the proposed dynamic behavior of atomic hydrogen species spilled on WO_3 (bottom).

Discussion

Based on the present *in situ* observations of the movements of H^+ and e^-, varying dynamic behaviors were found to take place during hydrogen spillover with differences even between reducible metal oxides, which have been considered promising platform materials. This section examines the manner in which these oxides affect the dynamics and reduction behavior of spilled atomic hydrogen and addresses the factors that allow hydrogen spillover to promote reduction (Figure 6). In the case of TiO_2 and WO_3, Zn^{2+} was reduced at approximately 100 °C under H_2 in the case that remote Pt was present to initiate hydrogen spillover. This promotional effect was derived from interparticle e^- diffusion accompanied by H^+ migration from Pt particles to remote Zn^{2+} ions. That is, hydrogen spillover on typical reducible metal oxides permits e^- diffusion as a consequence of the readily reducibility of the cations in such materials. In contrast, Zn^{2+} was reduced only above 300 °C under H_2 after Pt loading on MgO and CeO_2. In trials using MgO, Zn^{2+} was not reduced even though H^+ diffusion took place. It has been reported that e^- diffusion on non-reducible metal oxides is hindered because of the low reducibility of the associated cations.[26] Thus, the minimal reducing power of spilled hydrogen species on MgO can be attributed to a lack of e^- diffusion accompanying the H^+ diffusion. The reduction of Zn^{2+} by hydrogen spillover on CeO_2 did not occur at low temperatures even though both H^+ and e^- were found to diffuse on this material. This outcome was ascribed to the large activation energy for interparticle hydrogen spillover on CeO_2 (Figure 4b). Therefore, the retarded reduction of Zn^{2+} separated from Pt on CeO_2 is evidently a consequence of the inhibited interparticle hydrogen spillover.

The above results suggest two general insights concerning hydrogen spillover. Firstly, the reduction characteristics of spilled atomic hydrogen greatly depend on the dynamics of e^- diffusion rather than H^+ diffusion. Therefore, the reducibility of the platform material is a crucial factor to consider when hydrogen spillover is utilized for the reduction of metal ions. Secondly, there is possibility that hydrogen spillover is inhibited between interfaces even in the case of reducible metal oxides. Accordingly, it should be noted that interparticle hydrogen spillover is not always equivalent to intraparticle hydrogen spillover.

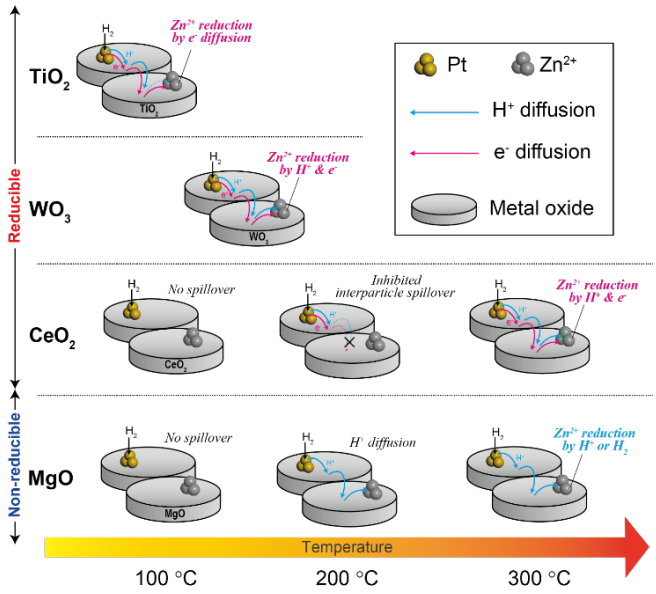

Figure 6. Proposed dynamic behaviors of spilled H^+ and e^- on each metal oxide platform at various temperatures and the associated effects on the reduction of Zn^{2+}.

Conclusions

The present work studied the hydrogen spillover phenomenon on typical metal oxides based on assessing the dynamics and reduction characteristics of H^+ and e^-. Based on systematic characterizations and analyses, a general and important insight on hydrogen spillover, the reduction characteristics of spilled atomic hydrogen are greatly affected by the e^- diffusion dynamics rather than by the H^+ diffusion properties of platform materials, was obtained. In this way, the e^- diffusion favorably occurs in conjunction with the H^+ diffusion on TiO_2 and WO_3 which significantly promotes the reduction of remote metal ions. On the other hand, the e^- diffusion coupled with H^+ is inhibited on MgO and CeO_2 due to its low reducibility or the difficultly in the interparticle diffusion which results in the retarded reduction of distant metal ions, respectively. These findings provide not only crucial insight on the dynamic behavior of spilled H^+ and e^- on various platform materials but also opportunity which promotes understanding of their reduction characteristics.

Experimental

Materials

$H_2PtCl_6{\cdot}6H_2O$ (≥98.5% pure) and $Zn(NO_3)_2{\cdot}6H_2O$ (≥99% pure) were purchased from Nacalai Tesque. JRC-TIO-6 [rutile TiO_2, Brunauer–Emmett–Teller (BET) surface area (S_{BET}) = 92.2 $m^2{\cdot}g^{-1}$] and JRC-CEO-2 (CeO_2, S_{BET} = 135.3) were both kindly supplied by the Catalyst Society of Japan. WO_3 (99.5% pure, S_{BET} = 5.5) and MgO (≥99% pure, S_{BET} = 2.5) were obtained from Wako Pure Chemical Industries, Ltd. All commercially-available chemicals were used as received.

Synthetic procedures

Pt/MO_x specimens used in this work (where MO_x = MgO, TiO_2, CeO_2 or WO_3) were synthesized using a conventional impregnation method. Briefly, $H_2PtCl_6{\cdot}6H_2O$ (0.0335 g) was added to a mixture of MO_x (1.0 g) and distilled water (100 mL) with stirring. The resulting suspension was further stirred at room temperature for more than 1 h after which the water was evaporated by heating the material at 60 ºC under vacuum to yield Pt/MO_x (containing 1.25 wt% Pt^{4+}). The Zn/MO_x specimens (containing 5 wt% Zn^{2+}) were obtained using $Zn(NO_3)_2{\cdot}6H_2O$ as the precursor via the same procedure employed to produce the Pt/MO_x. The Pt/MO_x and Zn/MO_x were grinded with an agate mortar at a 1:1 mass ratio for 3 min into a homogeneous powder prior to each trial to obtain the $(Pt + Zn)/MO_x$.

Characterization

TEM images were obtained with a field emission (FE) instrument (Hf-2000, Hitachi). H_2-temperature programmed reduction (TPR) analyses were conducted using a BEL-CAT instrument (MicrotracBEL Corp.). During these trials, 20 mg specimens were heated from 50 to 500 °C at rates of 2, 5 or 10 °/min under a 5.0% H_2/Ar flow. Prior to each H_2-TPR trial, a 5.0% H_2/Ar gas was dosaged to sample holder at 50 °C to stabilize TCD signal. Zn K-edge *in situ* X-ray absorption fine structure (XAFS) data were obtained in the transmission mode at the 01B1 beamline station within the SPring-8 facility operated by JASRI in Harima, Japan (proposal no. 2023A1933), employing a Si (111) monochromator. In a typical experiment, spectra were recorded while a pelletized sample was held in a batch-type *in situ* XAFS cell and heated at 5 °C/min from 50 to 400 °C under a 5.0% D_2/He flow. The resulting data were processed using the ATHENA program (Demeter). Diffuse reflectance infrared Fourier transform (DRIFT) spectra were obtained with a Bruker Vertex 70 instrument (Bruker Corp.) equipped with a CaF_2 window during the *in situ* XAFS analyses. *In situ* UV-visible spectra were acquired with a V-750 spectrometer (JACSO International Co., Ltd.) while heating specimens at a rate of 5 ºC/min from 50 to 400 °C under a H_2 flow.

Author Contributions

K.S. performed the characterization and wrote the manuscript. A.F. performed the catalyst preparation and helped the characterization. K.M. supervised the project. H.Y. helped supervise the project. The manuscript was written through the discussion with all authors. All authors have given approval to the final version of manuscript.

Data availability

The data that support the findings of this study are available from the corresponding author (K.M.) upon reasonable request.

Conflicts of interest

There are no conflicts to declare.

Acknowledgements

The present work was supported by Grants-in-Aid for Scientific Research (A24H003950 and T22K189200) from the Japan Society for the Promotion of Science (JSPS). K.S. thanks JSPS for a Research Fellowship for Young Scientists (no. 23KJ1506). The synchrotron radiation experiments providing XAFS and DRIFT data were performed at the BL01B1 beamline within the SPring-8 facility with the approval of JASRI (proposal no. 2023A1933).

Notes and references

1. S. Khoobiar, *J. Phys. Chem.*, 1964, **68**, 411-412.
2. M. Li, W. Yin, J. Pan, Y. Zhu, N. Sun, X. Zhang, Y. Wan, Z. Luo, L. Yi and L. Wang, *Chem. Eng. J.*, 2023, **471**, 144691.
3. R. Prins, *Chem. Rev.*, 2012, **112**, 2714-2738.
4. K. Shun, K. Mori, T. Kidawara, S. Ichikawa and H. Yamashita, *Nat. Commun.*, 2024, **15**, 6403.
5. A. Mahdavi-Shakib, T. N. Whittaker, T. Y. Yun, K. B. Sravan Kumar, L. C. Rich, S. Wang, R. M. Rioux, L. C. Grabow and B. D. Chandler, *Nat. Catal.*, 2023, **6**, 710-719.
6. R. Maeda, H. Sampei, R. Nakayama, T. Higo, Y. Koshizuka, Y. Bando, T. Komanoya, Y. Nakahara and Y. Sekine, *RSC Adv.*, 2024, **14**, 9869-9877.
7. C. Mao, J. Wang, Y. Zou, G. Qi, J. Y. Yang Loh, T. Zhang, M. Xia, J. Xu, F. Deng, M. Ghoussoub, N. P. Kherani, L. Wang, H. Shang, M. Li, J. Li, X. Liu, Z. Ai, G. A. Ozin, J. Zhao and L. Zhang, *J. Am. Chem. Soc.*, 2020, **142**, 17403-17412.
8. Q. Zhu, H. Zhou, L. Wang, L. Wang, C. Wang, H. Wang, W.

Fang, M. He, Q. Wu and F.-S. Xiao, *Nat. Catal.*, 2022, **5**, 1030-1037.
9. R. T. Yang and Y. Wang, *J. Am. Chem. Soc.*, 2009, **131**, 4224-4226.
10. N. Kostoglou, C.-W. Liao, C.-Y. Wang, J. N. Kondo, C. Tampaxis, T. Steriotis, K. Giannakopoulos, A. G. Kontos, S. Hinder, M. Baker, E. Bousser, A. Matthews, C. Rebholz and C. Mitterer, *Carbon*, 2021, **171**, 294-305.
11. Y. Li and R. T. Yang, *J. Am. Chem. Soc.*, 2006, **128**, 8136-8137.
12. S.-H. You, S.-M. Jung, K.-S. Kim, J. Lee, J. Park, H. Y. Jang, S. Shin, H. Lee, S. Back, J. Lee and Y.-T. Kim, *ACS Energy Lett.*, 2023, **8**, 2201-2213.
13. Q. He, L. Zeng, L. Han, M. M. Sartin, J. Peng, J.-F. Li, A. Oleinick, I. Svir, C. Amatore, Z.-Q. Tian and D. Zhan, *J. Am. Chem. Soc.*, 2021, **143**, 18419-18425.
14. J. Zhang, X. Liu, Y. Ji, X. Liu, D. Su, Z. Zhuang, Y.-C. Chang, C.-W. Pao, Q. Shao, Z. Hu and X. Huang, *Nat. Commun.*, 2023, **14**, 1761.
15. N. M. Briggs, L. Barrett, E. C. Wegener, L. V. Herrera, L. A. Gomez, J. T. Miller and S. P. Crossley, *Nat. Commun.*, 2018, **9**, 3827.
16. K. Shun, S. Matsukawa, K. Mori and H. Yamashita, *Small*, 2024, **20**, 2306765.
17. K. Mori, N. Hashimoto, N. Kamiuchi, H. Yoshida, H. Kobayashi and H. Yamashita, *Nat. Commun.*, 2021, **12**, 3884.
18. N. Hashimoto, K. Mori and H. Yamashita, *J. Phys. Chem. C*, 2023, **127**, 20786-20793.
19. K. Mori, K. Miyawaki and H. Yamashita, *ACS Catal.*, 2016, **6**, 3128-3135.
20. Y. Liu, R. Zhang, L. Lin, Y. Wang, C. Liu, R. Mu and Q. Fu, *Nat. Commun.*, 2023, **14**, 613.
21. M. D. Marcinkowski, A. D. Jewell, M. Stamatakis, M. B. Boucher, E. A. Lewis, C. J. Murphy, G. Kyriakou and E. C. H. Sykes, *Nat. Mater.*, 2013, **12**, 523-528.
22. T. Kamada, T. Ueda, S. Fukuura, T. Yumura, S. Hosokawa, T. Tanaka, D. Kan and Y. Shimakawa, *J. Am. Chem. Soc.*, 2023, **145**, 1631-1637.
23. W. Karim, C. Spreafico, A. Kleibert, J. Gobrecht, J. VandeVondele, Y. Ekinci and J. A. van Bokhoven, *Nature*, 2017, **541**, 68-71.
24. K. Shun, K. Mori, S. Masuda, N. Hashimoto, Y. Hinuma, H. Kobayashi and H. Yamashita, *Chem. Sci.*, 2022, **13**, 8137-8147.
25. A. Beck, P. Rzepka, K. P. Marshall, D. Stoian, M. G. Willinger and J. A. van Bokhoven, *J. Phys. Chem. C*, 2022, **126**, 17589-17597.
26. R. Prins, V. K. Palfi and M. Reiher, *J. Phys. Chem. C*, 2012, **116**, 14274-14283.
27. S. Masuda, K. Shun, K. Mori, Y. Kuwahara and H. Yamashita, *Chem. Sci.*, 2020, **11**, 4194-4203.
28. S. S. E. Collins, M. Cittadini, C. Pecharromán, A. Martucci and P. Mulvaney, *ACS Nano*, 2015, **9**, 7846-7856.
29. K. Motokura, *Chem. Asian J.*, 2024, e202301083.
30. C. Dong, R. Mu, R. Li, J. Wang, T. Song, Z. Qu, Q. Fu and X. Bao, *J. Am. Chem. Soc.*, 2023, **145**, 17056-17065.
31. T. Matsuda, R. Ishibashi, Y. Koshizuka, H. Tsuneki and Y. Sekine, *Chem. Commun.*, 2022, **58**, 10789-10792.
32. H. Kim, J. H. Park, J.-M. Ha and D. H. Kim, *ACS Catal.*, 2023, **13**, 11857-11870.
33. S. K. Beaumont, S. Alayoglu, C. Specht, N. Kruse and G. A. Somorjai, *Nano Lett.*, 2014, **14**, 4792-4796.
34. S. H. Park, M. S. Tzou and W. M. H. Sachtler, *Applied Catalysis*, 1986, **24**, 85-98.
35. S. Lee, H. Kim, R. Ryoo, J. Y. Park and M. Choi, *Nano Res.*, 2022, **15**, 10357-10365.
36. T. Whittaker, K. B. S. Kumar, C. Peterson, M. N. Pollock, L. C. Grabow and B. D. Chandler, *J. Am. Chem. Soc.*, 2018, **140**, 16469-16487.
37. S. Wang, Z.-J. Zhao, X. Chang, J. Zhao, H. Tian, C. Yang, M. Li, Q. Fu, R. Mu and J. Gong, *Angew. Chem. Int. Ed.*, 2019, **58**, 7668-7672.
38. Y. V. Larichev, B. L. Moroz and V. I. Bukhtiyarov, *Appl. Surf. Sci.*, 2011, **258**, 1541-1550.
39. H. Kang, L. Zhu, S. Li, S. Yu, Y. Niu, B. Zhang, W. Chu, X. Liu, S. Perathoner, G. Centi and Y. Liu, *Nat. Catal.*, 2023, **6**, 1062-1072.
40. Y. Yamazaki, T. Toyonaga, N. Doshita, K. Mori, Y. Kuwahara, S. Yamazaki and H. Yamashita, *ACS Appl. Mater. Interfaces*, 2022, **14**, 2291-2300.
41. D. A. Panayotov and J. T. Yates, *J. Phys. Chem. C*, 2007, **111**, 2959-2964.
42. D. A. Panayotov, S. P. Burrows, J. T. Yates, Jr. and J. R. Morris, *J. Phys. Chem. C*, 2011, **115**, 22400-22408.
43. Y. Yamazaki, K. Mori, Y. Kuwahara, H. Kobayashi and H. Yamashita, *ACS Appl. Mater. Interfaces*, 2021, **13**, 48669-48678.
44. N. Hashimoto, K. Mori, S. Matsuzaki, K. Iwama, R. Kitaura, N. Kamiuchi, H. Yoshida and H. Yamashita, *JACS Au*, 2023, **3**, 2131-2143.
45. J. Lee, P. Tieu, J. Finzel, W. Zang, X. Yan, G. Graham, X. Pan and P. Christopher, *JACS Au*, 2023, **3**, 2299-2313.
46. A. Beck, D. Kazazis, Y. Ekinci, X. Li, E. A. Müller Gubler, A. Kleibert, M.-G. Willinger, L. Artiglia and J. A. van Bokhoven, *ACS Nano*, 2023, **17**, 1091-1099.
47. C. Binet, M. Daturi and J.-C. Lavalley, *Catal. Today*, 1999, **50**, 207-225.
48. C. Binet, A. Badri and J.-C. Lavalley, *J. Phys. Chem.*, 1994, **98**, 6392-6398.
49. H. E. Kissinger, *Anal. Chem.*, 1957, **29**, 1702-1706.
50. Y. F. Li, N. Soheilnia, M. Greiner, U. Ulmer, T. Wood, F. M. Ali, Y. Dong, A. P. Yin Wong, J. Jia and G. A. Ozin, *ACS Appl. Mater. Interfaces*, 2019, **11**, 5610-5615.
51. J. Chen, C. Chen, M. Qin, B. Li, B. Lin, Q. Mao, H. Yang, B. Liu and Y. Wang, *Nat. Commun.*, 2022, **13**, 5382.
52. J. M. Kim, S. M. Chang, S. M. Kong, K.-S. Kim, J. Kim and W.-S. Kim, *Ceram. Int.*, 2009, **35**, 1015-1019.
53. H. Cheng, M. Wen, X. Ma, Y. Kuwahara, K. Mori, Y. Dai, B. Huang and H. Yamashita, *J. Am. Chem. Soc.*, 2016, **138**, 9316-9324.
54. C. Wang, E. Guan, L. Wang, X. Chu, Z. Wu, J. Zhang, Z. Yang, Y. Jiang, L. Zhang, X. Meng, B. C. Gates and F.-S. Xiao, *J. Am. Chem. Soc.*, 2019, **141**, 8482-8488.

TOC Graphics

The interparticle hydrogen spillover can be facilitated over TiO_2 and WO_3 as a consequence of the interfacial diffusion of H^+ and e^- pairs, while the e- diffusion coupled with H+ is inhibited on MgO and CeO_2.